MNRAS **000**, 1–9 (2015) Preprint 8 March 2016 Compiled using MNRAS LaTeX style file v3.0

Evidence for a binary origin of a central compact object.

Victor Doroshenko[1*], Gerd Pühlhofer[1], Patrick Kavanagh[1,2], Andrea Santangelo[1], Valery Suleimanov[1,3], Dmitry Klochkov[1]

[1]*IAAT, University of Tuebingen, Sand 1, Tuebingen, 72076, Germany*
[2]*School of Cosmic Physics, Dublin Institute for Advanced Studies, 31 Fitzwillam Place, Dublin 2, Ireland*
[3]*Kazan (Volga region) Federal University, Kremlevskaja str., 18, Kazan 420008, Russia*
[*]*E-mail: doroshv@astro.uni-tuebingen.de.*

arXiv:1508.03557v2 [astro-ph.HE] 7 Mar 2016

Accepted XXX. Received YYY; in original form ZZZ

ABSTRACT
Central compact objects (CCOs) are thought to be young thermally emitting isolated neutron stars that were born during the preceding core-collapse supernova explosion. Here we present evidence that at least in one case the CCO could have been formed within a binary system. We show that the highly reddened optical source IRAS 17287−3443, located $25''$ away from the CCO candidate XMMUJ173203.3−344518 and classified previously as a post asymptotic giant branch star, is indeed surrounded by a dust shell. This shell is heated by the central star to temperatures of $\sim 90\,\mathrm{K}$ and observed as extended infrared emission in 8-160 μm band. The dust temperature also increases in the vicinity of the CCO which implies that it likely resides within the shell. We estimate the total dust mass to be $\sim 0.4 - 1.5\,M_{\odot}$ which significantly exceeds expected dust yields by normal stars and thus likely condensed from supernova ejecta. Taking into account that both the age of the supernova remnant and the duration of active mass loss phase by the optical star are much shorter than the total lifetime of either object, the supernova and the onset of the active mass loss phase of the companion have likely occurred approximately simultaneously. This is most easily explained if the evolution of both objects is interconnected. We conclude, therefore, that both stars were likely members of the same binary system disrupted by a supernova.

Key words: stars: AGB and post-AGB – stars: neutron – binaries: general – stars: formation – ISM: supernova remnants

1 INTRODUCTION

Central compact objects (CCOs) are X-ray point sources without optical, radio, or pulsar wind nebula counterparts, found close to the centres of several young supernova remnants (SNRs). Their X-ray fluxes are constant within observational constraints and potential counterparts that would hint at accretion-dominated emission scenarios are not known. X-ray pulsations have been detected from three out of the eight CCOs known so far. All this suggests that CCOs are likely young $\leq 10^4$ yr isolated neutron stars (NSs), still cooling after their birth in a core-collapse supernova explosion (Pavlov et al. 2004; de Luca 2008). Measurements of the spin-down rates of pulsating CCOs imply very low dipole magnetic fields of the order of $10^{10} - 10^{11}$ G, compared to the regularly measured neutron star magnetic fields of $\sim 10^{12}$ G or to the even higher magnetic fields derived for magnetars. For this reason CCOs are sometimes dubbed “anti-magnetars” (Halpern & Gotthelf 2010a; Gotthelf et al. 2013). It is unknown, however, whether all of the CCOs are weakly magnetised, and whether they were born with these low magnetic fields.

In fact, detailed analysis of individual sources reveals CCOs as a rather diverse and intrinsically controversial sample. The high pulsed fractions observed in pulsating CCOs imply strong magnetic fields are necessary to explain non-uniform cooling of the NS surface (Bogdanov 2014). The long spin period (6.7 h) of the CCO candidate 1E 161348−5055 (Garmire et al. 2000) and superluminal echoes detected from Cas A (Krause et al. 2005) also favour magnetar-like CCO fields at those objects. Recently, Ho (2011) proposed that the dipole magnetic field of CCOs could have been “buried” during a hyper-accretion episode shortly after the supernova explosion. In this case different observational appearances of individual objects could be attributed to different properties of their birth environment.

Here we report the discovery of extended infrared emission towards the centre of the non-thermal shell-

© 2015 The Authors

type SNR G353.6−0.7 which hosts the CCO candidate XMMUJ173203.3−344518. We show that the observed emission is associated with dust heated by the optical source IRAS 17287−3443, previously classified by Suárez et al. (2006) as a post asymptotic giant branch (post-AGB) star. The large mass of dust in the shell suggests that the post-AGB wind is carving the proto-planetary nebula from material produced in the SN explosion and further supports the association with the SNR.

Both the SNR age and the duration of the active mass loss phase of the central star are much shorter than the lifetime of both objects, suggesting that the supernova explosion and the mass loss by the central star occurred approximately simultaneously. Such coincidence suggests that the evolution of two objects is likely interconnected which can only happen if both objects were members of the same binary system disrupted by the supernova explosion. We note that in this case the "buried" magnetic field scenario at the CCO is more likely to be realised as otherwise accreted material could only be supplied from the supernova ejecta.

2 EXTENDED INFRARED EMISSION

In this study, we used data products provided as part of the GLIMPSE (Churchwell et al. 2009) and MIPSGAL (Carey et al. 2009) surveys performed with the Infrared Array Camera (IRAC, 3.6-8 μm) and the Multi-band Imaging Photometer (MIPS, 24-160 μm) onboard the Spitzer space telescope. We also used public data (observations 1342214713, 1342214714) from the Photodetector Array Camera & Spectrometer (PACS, 70-160 μm) onboard the HERSCHEL space telescope, and XMM-Newton observations (0405680201, 0673930101, 0694030101, 0722090101, 0722190201) to image the SNR X-ray shell in the 0.2-10 keV energy range. Finally, we used Chandra ACIS-I data (observation 9139) for point source localisations. In all cases, we followed standard reduction procedures described in the respective instrument's documentation.

As part of an ongoing multi-wavelength analysis of the SNR emission, we inspected MIPSGAL maps covering the source. Immediately, the very peculiar extended structure coincident with the geometric centre of the X-ray SNR shell attracted our attention (see Fig. 1). Extended emission is detected across the 8 μm to 160 μm wavelength range, also in WISE and AKARI all-sky surveys. The highest luminosity is seen in the MIPS 24μm band. The extended emission region has a radius of $\sim 0\farcm5 - 2\farcm5$, and its surface brightness strongly peaks towards the bright inner $0\farcm5$ core, particularly at shorter wavelengths. In the IRAC 8 μm band, only the core is detected, and no extended emission is detected at shorter wavelengths. This strongly suggests that the warm dust with a temperature of ~ 90 K heated by a central source is responsible for the observed emission. We note that while collisional heating by hot shocked ejecta is normally expected to be an important ingredient in the thermal balance of dust residing within SNRs (Dwek et al. 2010), it is apparently not the case for G353.6-0.7.

Indeed, the temperature of the collisionally heated dust is expected to be defined by the temperature and density of hot ejecta and be fairly uniform throughout the SNR. However, as illustrated in Fig. 3, the observed dust temperature radial profile of the bright central shell is fully consistent with heating by the central source. Moreover, the observed X-ray emission from the remnant is known to be purely non-thermal and thus provides no observational evidence for presence of hot ejecta in this source (Acero et al. 2009; Bamba et al. 2012). We conclude, therefore, that heating by the central source dominates the dust thermal balance in the core of the shell. We note, however, that the heating efficiency of the central star decreases rapidly with distance, so collisional heating might still play some role in the outer parts of the remnant.

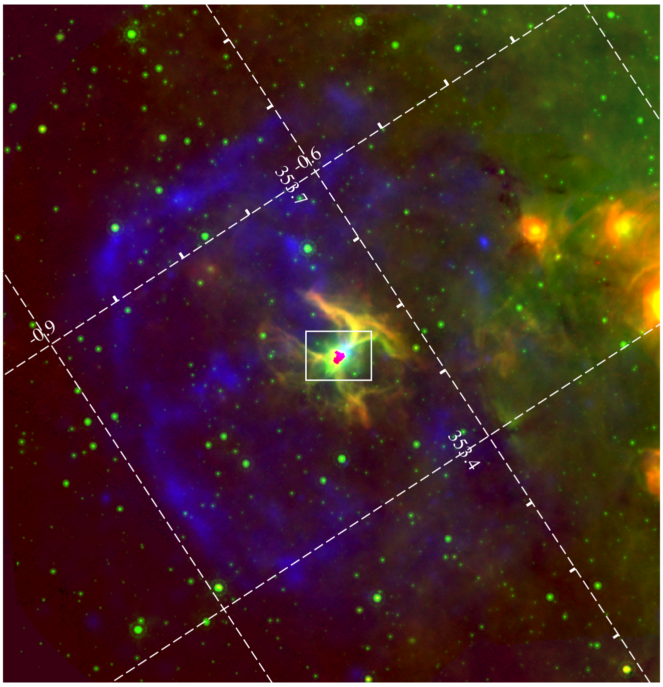

Figure 1. False-Colour X-ray and infrared emission image in the region around the SNR G353.6−0.7. The RGB colours correspond to HPACS 70 μm (red), MIPS 24 μm (green), and XMM-Newton 0.2-10 keV (blue) data, respectively. The intensity scale is logarithmic for all channels. The SNR shell in X-rays and the infrared dust shell are visible in the centre. The small box indicates the central part of the structure presented in Fig 2 in more detail. Galactic coordinates are also shown for reference.

A bright point source only slightly offset ($\sim 10''$) from the apparent geometrical centre of the extended structure is detected in the near-infrared, optical, ultraviolet (UV), and X-ray bands. We label it the "central star" (the object should not be confused with the CCO). It is the only bright source close to the centre of the extended emission and thus is likely the heating source for the dust. Analysis of the combined spectral energy distribution (SED) of the central star and the dust shell (see section 2.1) and of the observed dust's radial temperature profile (see Fig. 3 and appendix A1) strongly support this conclusion.

Two jet-like structures are clearly visible at 8 μm, extending from the central star in the direction perpendicular to the line connecting the star with the CCO, as illustrated in Fig. 2. These "jets" can also be traced at longer wavelengths. A second axis of symmetry, bisecting the outer "whiskers" visible in the 24 and 70 μm bands in the southeast-northwest

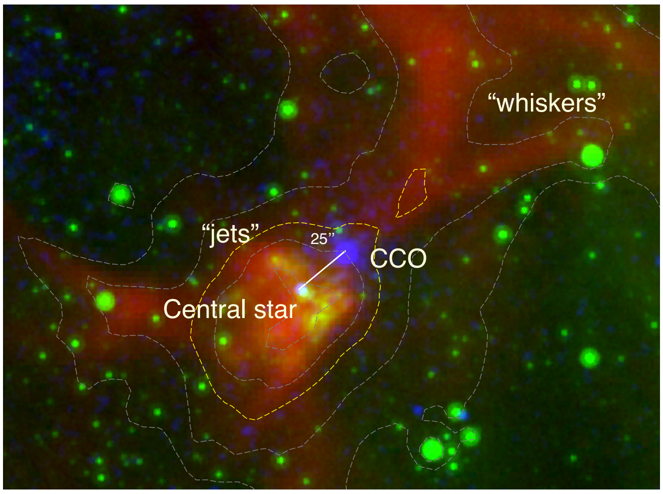

Figure 2. False-Colour X-ray and infrared emission image from the core of the infrared shell. The RGB colours correspond to Chandra X-ray 0.2-10 keV (blue), IRAC infrared 8 μm (green), and HPACS 70 μm (red) data. The intensity scale is logarithmic for all channels. Overlaid are equal brightness levels from the MIPS 24 μm band. Note that around the CCO the infrared emission is suppressed in the 70 μm band and enhanced in the 24 μm band suggesting higher dust temperature.

direction, also crosses the central star, as seen in Fig. 2. We conclude, therefore, that the morphology of the extended emission also supports an association with the central star.

Indeed, the CCO and the dust shell appear to be interacting. In particular, the infrared emission around the CCO is suppressed in the 70 μm band and enhanced in the 24 μm band as illustrated in Fig. 2. This strongly suggests additional heating of the dust by X-ray emission from the neutron star which can only be effective if the neutron star is submerged in the dust shell. The faint X-ray glow around the CCO, as visible in Fig. 2, has been shown to be inconsistent with pure point-source emission and indeed was interpreted by (Halpern & Gotthelf 2010b) as a dust-scattering halo around the CCO. We conclude, therefore, that the dust shell responsible for the observed infrared emission encloses both the CCO and the central star which heats the dust to the observed temperatures, and thus all three objects reside within the SNR shell. In the remaining sections we will demonstrate that all observed properties of the dust and the central source are consistent with this conclusion.

2.1 SED analysis

To obtain the SED of the central star, we used optical and near-infrared fluxes reported in the USNO-B (Monet et al. 2003) and 2MASS (Skrutskie et al. 2006) catalogues. In addition, data from the optical monitor onboard the XMM-Newton observatory were used to estimate fluxes in the ultraviolet band. The dust emission is dominated by the compact core and appears as a point source for most instruments, so as as a first approximation for the SED analysis of the extended emission, we used calibrated fluxes reported for IRAS 17287-3443 in the AKARI-FIS (Yamamura et al. 2009), the IRAS-PSC (Helou & Walker 1988), the MSX (Egan et al. 1999), and the WISE-PSC (Wright et al. 2010) catalogues. The combined SED for both the central star and the dust shell is presented in Fig. 3.

To describe the observed SED, we assumed blackbody-type emission subject to interstellar extinction (Fitzpatrick 1999) for the central star, whereas for the dust emission we used a modified blackbody model (Draine & Lee 1984) of the form $F_\lambda \sim \lambda^{-\beta} B_\lambda(T_{\rm dust})$. Here β is the dust emissivity index and $B_\lambda(T_{\rm dust})$ is the blackbody photon distribution (see also appendix A1 for details). The two components can be fit independently with best-fit temperatures of $T_* \geq 9000$ K for the optical star and $T_{\rm dust} \simeq 90$ K for the dust with an assumed typical grain size of 0.1μm and $\beta = 2$ (Planck Collaboration et al. 2014).

Strong intrinsic correlation between the temperature and the extinction coefficient together with high foreground absorption towards the source make the temperature (and thus luminosity) of the central star unconstrained from the fit even though the SED contains UV fluxes. This degeneracy can be resolved with additional assumptions on the extinction in the direction of the source. For instance, the extinction coefficient $A_V \sim 9$ can be estimated based on the observed X-ray absorption in the direction of the CCO (Acero et al. 2009; Tian et al. 2010; Halpern & Gotthelf 2010b; Klochkov et al. 2013), as detailed in appendix A2. This implies the luminosity of $\sim 6 \times 10^3\, L_\odot$ which, as discussed below, is sufficient to heat the dust to the observed temperature.

Comparison of the 8, 24, and 70 μm images implies that the dust temperature increases towards the centre of the shell, thus strongly suggesting heating by the central source. Modelling of the dust temperature or, equivalently, the observed flux ratio in the 24 and 70 μm as function of distance from the central source provides, therefore, another way to constrain its luminosity as described in appendix A1. In fact, simultaneous modelling the SEDs of the optical star and the dust together with the observed radial temperature profile (via the flux ratio in 24 and 70 μm bands) allows us to unambiguously relate the temperature of the central source and the dust grain size which remains the only unknown parameter. Note that in this case no assumptions on the extinction coefficient are required. However, we note that its best-fit value remains consistent with the estimate based on X-ray absorption for an assumed average grain size $a \sim$ 0.1μm, typical for cosmic dust. The results for this case are presented in Fig. 3 and Table 1.

Note that, as we show in section 3.1, the temperature and the luminosity of the central star are consistent with both the observed SED (under the assumption that the source is at the same distance as the SNR) and with the previous classification of the central source as a post-AGB core by Suárez et al. (2006) although detailed optical spectroscopy is required to unambiguously establish its spectral class. Therefore, we conclude that the SEDs of the dust and the central source are consistent with the hypothesis that the observed infrared emission comes from the dust shell heated by the central star located within the SNR.

3 DISCUSSION

3.1 Total dust mass

To understand the origin of the observed dust it is important to estimate its mass. In principle, for single-temperature dust

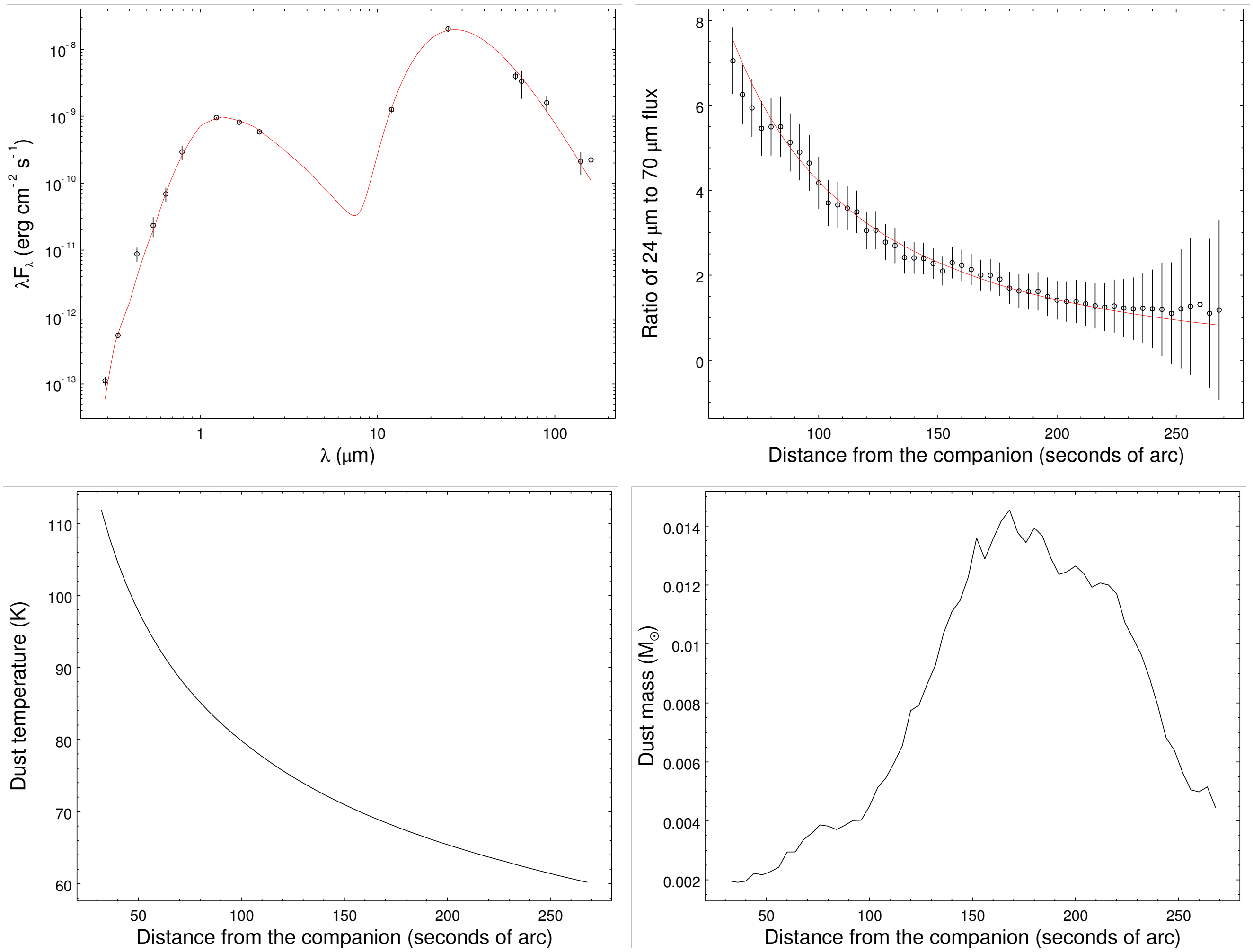

Figure 3. Top left: Combined broadband-SED of the central post-AGB star and its dust shell. Top right: Observed ratio of 24 to 70 μm fluxes as a function of the distance to the central star. The resulting radial distribution of the temperature (bottom left) and projected dust mass (bottom right) in the shell, estimated from the observed 24 and 70 μm fluxes, are shown for an assumed grain size of $a = 0.1\,\mu$m.

A_V	$T_*/1000\,\mathrm{K}$	$L_*/L_\odot$	T_dust	$M_\mathrm{dust}/M_\odot$	β
8.67(3)	91(5)	5788(25)	89(2)	0.4(1)	2.0(1)

Table 1. Best-fit parameters for the joint fit of the SED and radial temperature profile of the shell for an assumed grain size $a = 0.1\,\mu$m and ignoring projection effects. Uncertainties to last significant digit at 1σ confidence level are given in the parenthesis.

its mass can be estimated directly from the normalisation of the SED. However, given the observed temperature gradient away from the central star, a single temperature model is not justified. Indeed, the strong dependency of dust emissivity on temperature $L \sim < Q_{IR} > T^4$ implies that the colder outer regions do not contribute much to the observed flux, but might contain a large fraction of the total dust mass (here $< Q_{IR} >$ is the Planck-averaged dust emissivity for a given temperature). Therefore, we estimated the mass of the shell using the radial mass profile derived using observed radial flux profiles in the 24 μm and 70 μm bands under the assumption that the dust is in thermal equilibrium with the irradiating flux at each distance from the central star. The resulting projected dust mass profile for $a = 0.1\,\mu$m grains is presented in Fig. 3. Note that due to projection effects this figure may underestimate the total mass by up to an order of magnitude (see appendix A1).

The assumed grain size also strongly affects the estimated mass of the dust. In particular, grain sizes from $a = 1.5\,\mu$m to $a = 0.001\,\mu$m correspond to total dust masses between 0.03 and 50 $M_\odot$. Such a large uncertainty appears mainly because the SED of the central source does not allow us to constrain its reddening, effective temperature, and luminosity simultaneously. This degeneracy can be resolved through constraints on the central star's luminosity, either observational or theoretical. For instance, as discussed above, optical extinction can be estimated based on the observed X-ray absorption which would result in shell parameters close to those reported in Table 1.

Furthermore, temperatures and luminosities of real stars are not arbitrary and can be estimated based on stellar evolution considerations. For instance, if we assume that the central star is indeed going through a post-AGB phase, the luminosity can be constrained using the theoretical evolutionary tracks of post-AGB stars as presented in Fig. 4 for

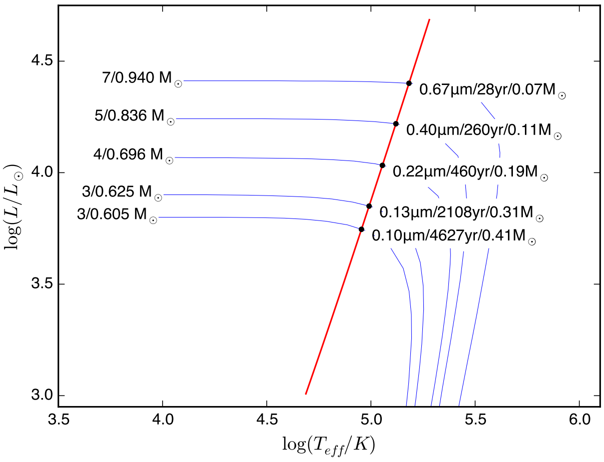

Figure 4. The temperature of the central source as derived from a combined SED and temperature profile analysis (red line), and evolutionary tracks of post-AGB stars with different masses. The dust grain size, the age of the star, and the total mass of the dust shell (for an assumed distance of 3.2 kpc) corresponding to each track are also shown.

several representative initial masses (Bloecker 1995). In the same figure, the temperature and luminosity of the central source required to explain the observed dust temperature profile is shown (based on the joint fitting of the SED and dust temperature profile as function of grain size acting as a free parameter).

Stars evolve along the tracks toward higher temperatures so the intersection of this line with evolutionary tracks not only implies a certain stellar luminosity, but also the time since the beginning of the AGB phase. Note that stars with large initial masses evolve too fast to survive long enough to explain both the observed infrared shell temperature and extent, so low luminosity tracks are preferred. This conclusion is also consistent with the relatively low observed X-ray luminosity of the central star (assuming the same X-ray to optical flux ratio as in other post-AGB stars (Ramstedt et al. 2012) of 10^{-5}). We would like to emphasise that evolutionary tracks with lower luminosities in this case also correspond to dust with a canonical grain size of $0.1\,\mu$m.

Note that different assumptions on distance to the source would not move the red line in Fig. 4 since these do not affect the dust temperature radial profile (see appendix 3.1). On the other hand, the derived dust mass and grain size do change, increasing and decreasing with the assumed distance for given luminosity, respectively. We conclude, therefore, that while the uncertainty in distance remains, both the SED of the central star and the dust temperature radial profile can be consistently modelled if dust consisting of $\sim 0.1\,\mu$m grains (which is typical for dust observed in the Galaxy) is heated by a low mass post-AGB star with age comparable to the age of the SNR.

This implies, however, that the dust must consist of grains with the average size of $0.1\,\mu$m, which corresponds to a total mass of dust in the shell of $\sim 0.4\,M_\odot$ ignoring projection effects (and up to 1.5-3 $M_\odot$ if these are taken into account, see appendix A1). This is at least two orders of magnitude more than dust yields expected from AGB stars which are between $10^{-5} - 10^{-2.5}\,M_\odot$ (Meijerink et al. 2003; Ventura et al. 2012), or, in fact, from any other known stars. There are several possibilities to explain this discrepancy.

First, the mass of the shell could be overestimated if the assumption that the dust is only heated by the central source does not hold. Inspection of the 8-70 μm images does indeed suggest that there is some emission in the North-Eastern and South-Western parts of the remnant outside of the inner dust shell, which seems to be spatially correlated with the diffuse X-ray emission from the SNR. Therefore, it is unlikely to be background emission. It also can not be dust heated by the central star due to large spatial distance separating them. In fact, such emission might be what one normally would expect to see within an SNR where the dust condensed from supernova ejecta is collisionally heated by cooling ejecta gas. However, the extended structure considered in our analysis is much brighter than anything else within the remnant and has a temperature distribution fully consistent with heating by a point source which thus dominates thermal balance of the dust.

On the other hand, past studies of dust formation in post-AGB atmospheres assumed that the dust condenses from the wind of an isolated star, expanding into the ISM. Apparently, this is not true for a star which was previously a member of a binary system which now resides inside the boundaries of an SNR containing metal-rich supernova ejecta. Indeed, conditions in winds of post-AGB stars are much less severe than those in supernova ejecta and are more suitable for dust condensation. However, atmospheres of AGB stars mostly consist of hydrogen which leads to comparatively low dust yields. Therefore, mixing of post-AGB wind with metal-rich material from supernova ejecta is likely to enhance overall dust production.

Finally, the dust contained in the proto-planetary nebula may not at all originate from the central star. Typically, the dust in proto-planetary nebulae has been pre-supplied during the intense mass-loss phase of the AGB star (Kwok 1993). However, SNe themselves are also prodigious formers of dust with masses of $> 0.5\ M_\odot$ possible in core-collapse ejecta, see e.g. Bianchi & Schneider (2007). Typically, the passage of the SNR reverse shock will destroy most, if not all, of the ejecta dust, (Nozawa et al. 2007). However, in the case of SNR G353.6−0.7, which is a purely non-thermal remnant in X-rays (H.E.S.S. Collaboration et al. 2011), we would not expect this to happen since non-thermal SNRs are thought to be evolving in very low-density bubbles blown by the progenitor massive star (Berezhko & Völk 2010), prohibitive to the formation of a strong reverse shock. Therefore, the majority of the dust could have survived to the current age. Assuming that wind from the central star has sufficiently high velocity, it can catch and shape some of this dust. Taking into account that the spatial size of the remnant exceeds that of the dust shell just by factor of three, this does not seem improbable. This scenario would offer further evidence for the association of the CCO and the central star. Note that in this case the central star is, in principle, not required to be an effective dust producer and must only have a sufficiently fast wind and high luminosity. These requirements are satisfied, for instance, by most WR stars. The classification of the central source as a post-AGB star by Suárez et al. (2006) seems, however, quite robust, and there is no apparent reason to question it even if the bulk of the dust is not condensed directly from stellar material.

3.2 Chance neighbours or relatives?

As discussed above, all observational facts point to the conclusion that the dust shell encloses both the CCO and the central star. Adopting the distance to the SNR of 3.2 kpc (H.E.S.S. Collaboration et al. 2011; Tian et al. 2010; Klochkov et al. 2013, 2015), the observed angular distance of $\sim 25''$ between the CCO and the central star implies a projected distance of just ~ 0.4 pc between the two objects[1]. The average density of AGB-stars in the Galaxy is $\sim 1\,\mathrm{kpc}^{-3}$ (Jackson et al. 2002), so the probability that the two objects are chance neighbours is very low. Given the nature and the recent history of the two objects, the hypothesis that they were members of the same binary system before the supernova explosion of the CCO's progenitor star is immediately very suggestive.

This conclusion is indirectly supported by the observed morphology of the infrared emission. Indeed, the jet-like structures seen at shorter wavelengths form a clear axis of symmetry resembling the one seen in bipolar planetary nebulae (Dobrinčić et al. 2008), which are usually associated with collimation of outflowing wind due to orbital motion in a binary system (Solf & Ulrich 1985). Another symmetry axis perpendicular to the jets bisects the outer "whiskers" and passes directly through the CCO. This is highly unlikely to be simply by chance or due to projection effects, but can be explained if the two objects were in the past members of a binary system destroyed by a supernova explosion. The observed $25''$ offset between the central star and the CCO is consistent with this hypothesis. Assuming that the supernova explosion happened ~ 4.5 kyr ago implies that the two stars move away from each other with a projected velocity of $\sim 100\,\mathrm{km\,s}^{-1}$, which is not unreasonable.

Moreover, the ages of the infrared structure and the SNR shell must be comparable. Indeed, we already discussed that if the central source is a post-AGB star it must have entered the mass loss phase quite recently. Furthermore, terminal wind velocities of massive stars are usually below $1000\,\mathrm{km\,s}^{-1}$, therefore the $5'$ extension measured for the infrared shell implies a lower age limit of ~ 4500 yr consistent with the existing estimates for the SNR's age (Yang et al. 2014). On the other hand, both the post-AGB phase of the central star and the X-ray bright phase of the SNR are expected to have relatively short lifetimes ($\lesssim 10000$ yr), limiting the maximum ages of both objects. Given that the total lifetime of both stars is much longer than 10 kyr, such coincidence is unlikely unless their evolutionary paths are interconnected, i.e. they were members of the same binary system disrupted by a supernova explosion ~4-10 kyr ago. In this case, either the supernova explosion could have been triggered by the enhanced mass transfer from the companion which entered the AGB phase or vice-versa.

3.3 Accretion onto the neutron star

The "buried field" scenario proposed by Ho (2011) to explain apparently low magnetic fields of the CCOs invokes a powerful accretion episode soon after the supernova explosion. Mass loss rates of AGB stars can reach $\sim 10^{-4} M_\odot\,\mathrm{yr}^{-1}$ (Meijerink et al. 2003), and although the current distance between the central star and the CCO implies that the plasma density in the vicinity of the neutron star is too low to explain the observed X-ray luminosity of $10^{34}\,\mathrm{erg\,s}^{-1}$ by accretion of this material onto the neutron star, the situation could have been quite different in the past.

Indeed, accretion at much higher rates should have been possible when the neutron star was closer to its former companion and was thus submerged in the much denser and slower wind, or even in a common envelope surrounding the former binary components. In the latter case, accretion rates of up to $10^{-3} M_\odot\,\mathrm{yr}^{-1}$ (Chevalier 1993) can be expected. Indirect evidence that powerful accretion did indeed take place in the past comes from the fact that XMMUJ173203.3−344518 is the most luminous CCO known to date, despite not being the youngest. This suggests that it must have also been heated after the supernova explosion, likely due to accretion. Moreover, as discussed above, the gap between the outer "whiskers" visible in the 24-70 μm images is perfectly aligned with the line connecting the central source and the CCO. This can naturally be explained if the dust was destroyed by strong X-ray emission from the neutron star during its early high-accretion rate state. This can also be the reason for the overall asymmetric shape of the extended emission. The proposed model to explain the observational evidence is thus that the neutron star was indeed accreting at high rates in the past, shortly after the supernova explosion. This would imply that the system exhibits the first observational evidence for the "buried magnetic field" scenario proposed by Ho (2011) to explain the slow spin evolution of CCOs.

4 CONCLUSIONS

We report on the discovery of the infrared shell surrounding a post-AGB star projected at the geometrical centre of the supernova remnant G353.6−0.7. Based on the analysis of infrared data, we conclude that the observed emission comes from a dust shell heated by the central star likely located within the supernova remnant. Furthermore, additional dust heating by the CCO suggests that the shell encloses both the central star and the CCO and, therefore, resides within the supernova remnant. Based on the morphology of the infrared shell and comparison of its evolutionary timescale with that of the SNR, we conclude that the post-AGB star and the progenitor of the remnant's CCO were likely members of the same binary system disrupted by the supernova explosion. This could be the first evidence for a binary origin of a CCO. We note that, in this case, accretion of metal-rich material onto the neutron star early on after the supernova explosion could explain the slow spin evolution of CCOs via the "buried field" scenario and high carbon content in the atmosphere of the neutron star.

---

[1] Distances well beyond the Galactic centre are strongly disfavoured since they would imply an unrealistically large CCO radius (Klochkov et al. 2013, 2015), and also a TeV luminosity of the SNR by far exceeding that of other similar sources (Acero et al. 2015). A distance at 5-6 kpc (Fukuda et al. 2014) would not change our conclusions.

In addition, we estimated the mass of the dust in the shell and concluded that it significantly exceeds the expected dust yield from the central post-AGB star and is closer to that from the supernova. This suggests that the interaction of the central stars' wind with the ejecta enhances the dust formation in central parts of the remnant. We note that a significant fraction of all core-collapse supernovae are expected to occur in binary systems, often with medium sized companions, which have similar evolutionary paths as the central star in SNR G353.6−0.7. The contribution of such systems to the Galactic dust budget has not been assessed thus far, and, given the large estimated dust mass around the central star in SNR G353.6−0.7, could be an important dust formation mechanism.

ACKNOWLEDGEMENTS

The authors thank Emma Whelan and Klaus Werner for their very useful comments. The authors acknowledge support from Deutsches Zentrum für Luft- und Raumfahrt (DLR) through DLR-PT grants 50 OR 1310 and 50 OR 0702, from Deutsche Forschungsgemeinschaft (DFG) through grants DFG WE 1312/48-1 and Emmy Noether research grant SA2131/1-1, from Bundesministerium für Bildung und Forschung (BMBF) through DESY-PT grant 05A14VT1, and from the European Space Agency PRODEX Programme - Contract Number 420090172. This work is based in part on archival data obtained with the Spitzer Space Telescope, which is operated by the Jet Propulsion Laboratory, California Institute of Technology under a contract with NASA. This work also made use of Hershel and XMM-newton data. Herschel is an ESA space observatory with science instruments provided by European-led Principal Investigator consortia and with important participation from NASA. XMM-Newton is an ESA science mission with instruments and contributions directly funded by ESA Member States and NASA. This publication makes use of data products from the Wide-field Infrared Survey Explorer, which is a joint project of the University of California, Los Angeles, and the Jet Propulsion Laboratory/California Institute of Technology, funded by the National Aeronautics and Space Administration. This research has also made use of the NASA/IPAC Infrared Science Archive (IRSA), which is operated by the Jet Propulsion Laboratory, California Institute of Technology, under contract with the National Aeronautics and Space Administration. All infrared data used in this work is available through IRSA.

REFERENCES

Acero F., Pühlhofer G., Klochkov D., Komin N., Gallant Y., Horns D., Santangelo A., for the H. E. S. S. Collaboration 2009, preprint, (`arXiv:0907.0642`)

Acero F., Lemoine-Goumard M., Renaud M., Ballet J., Hewitt J. W., Rousseau R., Tanaka T., 2015, A&A, 580, A74

Bamba A., et al., 2012, ApJ, 756, 149

Berezhko E. G., Völk H. J., 2010, A&A, 511, A34

Bianchi S., Schneider R., 2007, MNRAS, 378, 973

Bloecker T., 1995, A&A, 299, 755

Bogdanov S., 2014, ApJ, 790, 94

Carey S. J., et al., 2009, PASP, 121, 76

Chevalier R. A., 1993, ApJl, 411, L33

Churchwell E., et al., 2009, PASP, 121, 213

Dobrinčić M., Villaver E., Guerrero M. A., Manchado A., 2008, AJ, 135, 2199

Draine B. T., Lee H. M., 1984, ApJ, 285, 89

Dwek E., et al., 2010, ApJ, 722, 425

Egan M. P., Price S. D., Shipman R. F., Gugliotti G. M., Tedesco E. F., Moshir M., Cohen M., 1999, in Bicay M. D., Cutri R. M., Madore B. F., eds, Astronomical Society of the Pacific Conference Series Vol. 177, Astrophysics with Infrared Surveys: A Prelude to SIRTF. p. 404

Fitzpatrick E. L., 1999, PASP, 111, 63

Fukuda T., Yoshiike S., Sano H., Torii K., Yamamoto H., Acero F., Fukui Y., 2014, ApJ, 788, 94

Garmire G. P., Pavlov G. G., Garmire A. B., Zavlin V. E., 2000, IAU Circ., 7350, 2

Gotthelf E. V., Halpern J. P., Alford J., 2013, ApJ, 765, 58

H.E.S.S. Collaboration et al., 2011, A&A, 531, A81

Halpern J. P., Gotthelf E. V., 2010a, ApJ, 709, 436

Halpern J. P., Gotthelf E. V., 2010b, ApJ, 710, 941

Helou G., Walker D. W., eds, 1988, Infrared astronomical satellite (IRAS) catalogs and atlases. Volume 7: The small scale structure catalog

Ho W. C. G., 2011, MNRAS, 414, 2567

Jackson T., Ivezić Ž., Knapp G. R., 2002, MNRAS, 337, 749

Klochkov D., Pühlhofer G., Suleimanov V., Simon S., Werner K., Santangelo A., 2013, A&A, 556, A41

Klochkov D., Suleimanov V., Pühlhofer G., Yakovlev D. G., Santangelo A., Werner K., 2015, A&A, 573, A53

Krause O., et al., 2005, Science, 308, 1604

Kwok S., 1993, ARA&A, 31, 63

Laor A., Draine B. T., 1993, ApJ, 402, 441

Meijerink R., Mellema G., Simis Y., 2003, A&A, 405, 1075

Monet D. G., et al., 2003, AJ, 125, 984

Nozawa T., Kozasa T., Habe A., Dwek E., Umeda H., Tominaga N., Maeda K., Nomoto K., 2007, ApJ, 666, 955

Pavlov G. G., Sanwal D., Teter M. A., 2004, in Camilo F., Gaensler B. M., eds, IAU Symposium Vol. 218, Young Neutron Stars and Their Environments. p. 239 (`arXiv:astro-ph/0311526`)

Planck Collaboration et al., 2014, A&A, 564, A45

Ramstedt S., Montez R., Kastner J., Vlemmings W. H. T., 2012, A&A, 543, A147

Skrutskie M. F., et al., 2006, AJ, 131, 1163

Solf J., Ulrich H., 1985, A&A, 148, 274

Suárez O., García-Lario P., Manchado A., Manteiga M., Ulla A., Pottasch S. R., 2006, A&A, 458, 173

Tian W. W., Li Z., Leahy D. A., Yang J., Yang X. J., Yamazaki R., Lu D., 2010, ApJ, 712, 790

Ventura P., et al., 2012, MNRAS, 424, 2345

Vuong M. H., Montmerle T., Grosso N., Feigelson E. D., Verstraete L., Ozawa H., 2003, A&A, 408, 581

Wright E. L., et al., 2010, AJ, 140, 1868

Yamamura I., et al., 2009, in Onaka T., White G. J., Nakagawa T., Yamamura I., eds, Astronomical Society of the Pacific Conference Series Vol. 418, AKARI, a Light to Illuminate the Misty Universe. p. 3

Yang R.-z., Zhang X., Yuan Q., Liu S., 2014, A&A, 567, A23

de Luca A., 2008, in Bassa C., Wang Z., Cumming A., Kaspi V. M., eds, American Institute of Physics Conference Series Vol. 983, 40 Years of Pulsars: Millisecond Pulsars, Magnetars and More. pp 311–319 (`arXiv:0712.2209`), doi:10.1063/1.2900173

APPENDIX A: APPENDIX

A1 Dust mass and thermal balance.

The infrared flux from the dust envelope observed at Earth can be approximated as

$$\lambda F_\lambda = \frac{2\pi a^2 N}{4\pi D^2} Q_{IR}(a,\lambda) \frac{2hc^2/\lambda^4}{(e^{hc/\lambda k T_{\rm dust}} - 1)}$$

where D is the distance to the source, $Q_{IR} \simeq (2\pi a/\lambda)^\beta$ is the dust emissivity of grains with size a at a given wavelength (Draine & Lee 1984) and N is the total number of dust grains. The dust mass $M_{\rm dust} = 4/3\pi a^3 \rho N$ can, therefore, be estimated from the observed flux if the grain size and density ρ are known or assumed. The problem is, however, that the emissivity index β and grain parameters are generally not known, which strongly affects the estimated dust temperature and mass. On the other hand, dust only emits because it is heated by an external source. To within an order of magnitude, the thermal balance of dust grains in an external radiational field at given distance d_* from the heating source can be described as

$$L_*(T_*)/4\pi d_*^2 < Q_{UV}(T_*) >= 4 < Q_{IR}(T_{\rm dust}) > \sigma_B T_{\rm dust}^4$$

where L_*, T_* are its luminosity and effective temperature, $T_{\rm dust}$ is the dust temperature, and $< Q_{IR} >$ and $< Q_{UV} >$ are the Planck-averaged dust emission and absorption cross-sections (Draine & Lee 1984). For a given emissivity law (i.e. emissivity index β), the observed dust temperature at a given distance can be estimated using the ratio of 24 and 70μm fluxes. On the other hand, β can be constrained using the broadband SED. In fact, the situation is more complicated due to the dependence of $< Q_{IR} >, < Q_{UV} >$, and β on temperature, so the observed flux ratio must be modelled simultaneously with the broadband SED to obtain a self-consistent solution.

We measured the radial flux profiles in the 24 and 70μm bands using a set of circular annuli with radii from 60$''$ to 270$''$ and a width of 4$''$, centred on the central source as shown in Fig. A1. We excluded the inner 1$'$ core from the fit due to saturation of MIPS data and a potentially complex structure due to presence of the "jets" and additional heating of the dust by X-rays from the neutron star. From the observed fluxes we subtracted the background measured in the outer annulus with a radius of 270-350$''$, where no source emission is apparent. We also included a systematic error of 5% to account for absolute flux calibration uncertainties of both MIPS and PACS and included a temperature-dependent colour correction as described in the respective instruments' documentation, to calculate the expected fluxes for a given temperature. We also assumed a distance to the object from Earth of 3.2 kpc, and an astronomical silicate dust composition with cross-sections from (Draine & Lee 1984; Laor & Draine 1993). We would like to emphasise here that thermal balance equation itself does not depend on the assumed distance to the source D. Indeed, the observed luminosity of the central source $L_* \propto F_{\rm obs,bol} D^2$ has the same dependence on distance as the physical distance from grains to the central source $d_*^2 \propto (\alpha D)^2$. However, the observed bolometric flux $F_{\rm obs,bol}$ is uncertain due to strong reddening of the optical star. Therefore, either extinction coefficient or distance to the source have to be assumed to constrain the luminosity of the source. We verified also that the main results are not changed if a carbon composition as provided by the same authors is assumed. Calculated flux ratios were then compared to the observed values by simultaneously fitting the flux ratio profile and the SED. Once the parameters of the fit are fixed, the dust mass in each radial region can be calculated from the respective normalisation in the same way as for the SED.

Note that we ignored the projection effects as the true geometry of the shell is not known. Dust can be considered optically thin in the infrared, so fluxes measured within annular regions represent, in effect, a combination of emission from individual spherical shells defined by corresponding annular extraction regions. The contribution of each shell to the flux measured in a given region is proportional to the volume occupied by dust within the intersection between the respective spherical shell and annular cylinder. In principle, knowledge of the three-dimensional structure of the shell is, therefore, required to model the observed emission. However, a strong dependence of the total flux on temperature and fast drop of temperature with distance to the heating source imply that the contribution of outer annuli to the flux measured from a given region is negligible. Indeed, even without accounting for projection effects the observed flux ratio in the 24 and 70 μm bands is consistent with the predicted radial temperature profile.

However, projection directly affects the dust mass estimate. It is trivial to show that the volume of intersection between the co-centric spherical shell and annular cylinder relative to the total volume of the respective spherical shell is $V_{\rm x}/V_{shell} = (r_o^2 - r_i^2)^{1.5}/(r_o^3 - r_i^3)$, where r_o, r_i are the outer and inner radii of the shell. For regions we used to estimate the temperature profile, these are $0.3 - 0.1$, for the inner and outer parts of the shell, respectively. Together with the dust mass estimated using the flux in individual regions, this implies that by ignoring projection effects we underestimate the total dust mass by a factor of ~ 7. Note, however, that the observed morphology of the infrared emission implies that the dust shell is clearly not spherically symmetric, so in reality this factor shall probably be a factor of two lower, which implies the dust mass of $1.5 M_\odot$ for the preferred solution with grain size of $a = 0.1\,\mu$m.

A2 X-ray absorption column and extinction.

The expected optical extinction coefficient can be calculated from the X-ray absorption column as $A_V \simeq N_H/1.6\times10^{21}$ (Vuong et al. 2003). Based on the X-ray spectrum of the CCO, an absorption column of $(1.4-1.9)\times10^{22}$ has been reported by (Klochkov et al. 2015), which translates to $A_V \sim 8.7 - 12$ and agrees well with the value obtained from the SED fit ($A_V = 8.67$).

A3 X-ray emission from the central star.

The central source is detected in X-rays as well (see Fig. 2). Based on the *Chandra* X-ray spectrum, its flux is estimated to $\sim 10^{-13}\,{\rm erg\,cm^{-2}\,s^{-1}}$, corresponding to a luminosity of $L_x \sim 10^{32}\,{\rm erg\,s^{-1}}$ (adopting the absorption column of $N_H \sim 1.4\times10^{22}$ (Klochkov et al. 2015) and a blackbody spectrum with a best-fit temperature of $\sim 3\times10^6$ K). We omitted this measurement in the SED modelling since the hard X-ray emission of X-ray active stars is believed to be non-photospheric, but rather due to either enhanced coronal

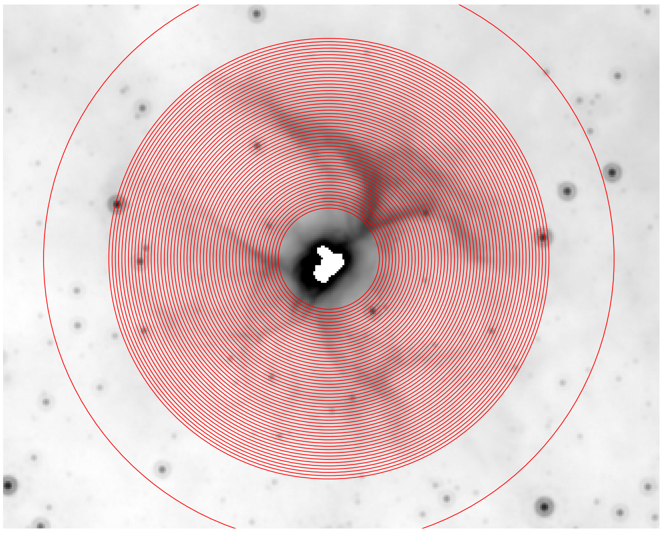

Figure A1. Regions used to measure the radial flux profiles in the 24 μm and 70 μm bands (the MIPS 24 μm image is shown for reference). The contribution of point sources was excluded from each image. The outer region was used to estimate the background.

activity or strong shocks in stellar winds. The ratio of the X-ray to optical luminosity is consistent with values typically observed from X-ray active AGB stars (Ramstedt et al. 2012). Thus, we considered the detection of X-rays from the central source as an additional argument to support the classification of IRAS 17287-3443 as a post-AGB star.

This paper has been typeset from a TEX/LATEX file prepared by the author.